

Quantum circuit architecture search: error mitigation and trainability enhancement for variational quantum solvers

Yuxuan Du,¹ Tao Huang,² Shan You,² Min-Hsiu Hsieh,³ and Dacheng Tao¹

¹*UBTECH Sydney AI Centre, School of Computer Science,
Faculty of Engineering, The University of Sydney, Australia*

²*SenseTime*

³*Centre for Quantum Software and Information,
Faculty of Engineering and Information Technology, University of Technology Sydney, Australia*

(Dated: December 2, 2021)

Quantum error mitigation techniques are at the heart of quantum computation. Conventional quantum error correction codes are promising solutions, while they become infeasible in the noisy intermediate scale quantum (NISQ) era, hurdled by the required expensive resources. The variational quantum learning scheme (VQLS), which is composed of trainable quantum circuits and a gradient-based classical optimizer, could partially adapt the noise affect by tuning the trainable parameters. However, both empirical and theoretical results have shown that for most variational quantum algorithms, noise can deteriorate their performances evidently when the problem size scales. Furthermore, VQLS suffers from the barren plateau phenomenon. Here we devise a resource and runtime efficient scheme, i.e., quantum architecture search scheme (QAS), to better improve the robustness and trainability of VQLS. Particularly, given a learning task, QAS actively seeks an optimal architecture among all possible circuit architectures to balance benefits and side-effects brought by adding quantum gates, where more quantum operations enable a stronger expressive power of the quantum model but introduce a larger amount of noise and more serious barren plateau scenario. To this end, QAS implicitly learns a rule that can well suppress the influence of quantum noise and the barren plateau. We implement QAS on both the numerical simulator and real quantum hardware via the IBM cloud to accomplish the data classification and the quantum ground state approximation tasks. Numerical and experimental results exhibit that QAS outperforms conventional variational quantum algorithms with heuristic circuit architectures. Our work provides guidance for developing advanced learning based quantum error mitigation techniques on near-term quantum devices.

I. Introduction

Quantum error mitigation is an indispensable technique to realize the large scale quantum computation [1, 2]. During the past decades, a huge effort has been dedicated to devising various quantum error correction codes such as surface code and toric code to detect and correct errors caused by decoherence and imperfect control [3–5]. However, the implementation of these quantum error correction protocols requests expensive quantum resources, including a large number of ancillary qubits and multi-control quantum gates, which are prohibitive to noisy intermediate scale quantum (NISQ) devices [2]. To this end, resource efficient alternatives have been widely explored to mitigate error in NISQ machines. A representative direction to suppress the noise effect is quasi-probability strategies [6, 7]. Concretely, attributed to the linearity of quantum mechanics, a linear combination of noisy circuits with suitable coefficients can achieve probabilistic error cancellation and then return a noiseless quantum circuit when the knowledge of the error distribution is accessible. Although this approach is resource efficient without using ancillary qubits, its scalability is limited, since capturing the error distribution of a large quantum system is intractable. Beyond quasi-probability approaches, several studies have revisited the error mitigation as a learning problem [8, 9], whereas the proposed algorithms can only

suppress noise for the Clifford quantum circuit that can be efficiently simulated by classical computers [10]. A general quantum error mitigation technique that is both runtime and resource efficient remains largely unknown.

Variational quantum learning scheme (VQLS) [11], which is also known as the quantum neural network [12–14], is one of the most promising candidates to use NISQ devices to solve practical tasks beyond the reach of classical computers. For example, a recent study has implemented a variational Eigen-solver on the Sycamore quantum processor to model the binding energy of the hydrogen chains [15]. The success of VQLS mainly origins from its flexible mechanism. Recall the paradigm of VQLS. Given a learning task, VQLS employs a gradient-based classical optimizer to continuously update parameters in trainable quantum circuits $U(\boldsymbol{\theta})$ to minimize a predefined objective function \mathcal{L} [16, 17]. Mathematically, VQLS aims to find the optimal $\boldsymbol{\theta}^*$ by minimizing the objective function \mathcal{L} within a certain constraint set $\mathcal{C} \subseteq \mathbb{R}^d$, i.e.,

$$\boldsymbol{\theta}^* = \arg \min_{\boldsymbol{\theta} \in \mathcal{C}} \mathcal{L}(\boldsymbol{\theta}, \mathbf{z}), \quad (1)$$

where the input \mathbf{z} and the form of \mathcal{L} depend on specific tasks. For instance, when VQLS is specified as an Eigen-solver [11], \mathbf{z} refers to a Hamiltonian and the objection function yields $\mathcal{L} = \text{Tr}(\mathbf{z} |\psi(\boldsymbol{\theta})\rangle \langle \psi(\boldsymbol{\theta})|)$, where $|\psi(\boldsymbol{\theta})\rangle$ is the quantum state generated by $U(\boldsymbol{\theta})$. Analogous to deep neural networks [18], the trainable quantum circuit $U(\boldsymbol{\theta})$

in VQLS generally adopts a multi-layer architecture, i.e.,

$$U(\boldsymbol{\theta}) = \prod_{l=1}^L U_l(\boldsymbol{\theta}), \quad (2)$$

where $U_l(\boldsymbol{\theta})$ is composed of a sequence of parameterized single qubit and two qubits quantum gates, and $\boldsymbol{\theta}$ are adjustable parameters of quantum gates. Note that the arrangement of quantum gates in $U_l(\boldsymbol{\theta})$ is flexible, which enables VQLS to adequately utilize the available quantum resources and adapt any physical implementation restriction. Moreover, in the training process, the classical optimizer can exploit the received noisy information to update parameters $\boldsymbol{\theta}$ to minimize the objective function \mathcal{L} . In other words, VQLS, as with deep neural networks, is robust to a small amount of noise [19–21]. However, both theoretical and experimental studies showed that the performance of VQLS suffers from the barren plateau phenomenon, where the gradient can be exponentially vanished and full of noise with respect to the increased circuit depth, the number of qubits, and the amount of noise [22–25]. Therefore, to guarantee the performance of VQLS for large scale problems, it is necessary to introduce an effective technique to further improve the trainability of VQLS. Namely, the error mitigation and *trainability* enhancement amount to inhibiting the noise affect and the barren plateau to enable that the result $\mathcal{L}(\boldsymbol{\theta}^{(T)})$ returned by VQLS is close to the optimal result $\mathcal{L}(\boldsymbol{\theta}^*)$.

The design of a technique that can achieve error mitigation and trainability enhancement for VQLS is challenging. The fundamental difficulty is that under the NISQ setting, involving more quantum resources into the trainable quantum circuits $U(\boldsymbol{\theta})$ will result in both positive and negative aftermath. In particular, the expressive power of $U(\boldsymbol{\theta})$ will be strengthened by increasing the number of layers L such that the hypothesis class represented by $U(\boldsymbol{\theta})$ is enlarged [16, 17]. Meanwhile, a deep circuit depth implies that the gradient information received by the classical optimizer is exponentially vanished and full of noise, because of the barren plateau phenomenon and the accumulated gate noise. In other words, deep circuit depth may render the optimization to be diverged [23, 24]. Under the above observations, the error mitigation and the trainability enhancement in VQLS amount to seeking a circuit architecture that utilizes the least quantum resources to implement $U(\boldsymbol{\theta})$ that covers the target concept. However, locating such an architecture is computationally hard, since the searching space of possible architectures scales exponentially with respect to the number of qubits and the circuit depth. Furthermore, quantum gates are accompanied by varied amounts of noise, e.g., two qubits gates are much noisier than single qubit gates. Incorporating such weighted noise further exacerbates the difficulty of the error mitigation design for VQLS. Last, the proposed method should possess high compatibility with physical restrictions, since the qubits connectivity and the types of available quantum gates for different quantum devices are not unified.

To address all concerns aforementioned, here we devise a quantum architecture search scheme (QAS) to accomplish the error mitigation and the trainability enhancement towards variational quantum algorithms. The advance of QAS is ensured by reformulating the error mitigation and the alleviation of the barren plateau in VQLS as a learning problem. Notably, QAS does not request any ancillary quantum resource and its runtime is almost the same with the conventional VQLS. In addition, QAS is compatible with all quantum platforms, e.g., optical, trapped-ion, and superconducting quantum machines, since it can actively adapt physical restrictions and weighted noise of varied quantum gates. Moreover, QAS can be seamlessly integrated with other quantum error mitigation methods and barren plateau solutions [6, 7, 26]. Celebrated by the universality and efficacy, QAS contributes to a broad class of variational quantum algorithms built on various quantum machines. To the best of our knowledge, this is the first proposal that can be directly applied to current quantum machines to achieve the error mitigation and the trainability enhancement with scalability. Remarkably, QAS can be further applied to other tasks beyond VQLS, which includes the exploration of optimal quantum control protocols and the approximation of the target unitary using the available quantum gates.

II. The quantum architecture search

Let us formalize the error mitigation and the trainability enhancement for VQLS as a learning task. Denote \mathcal{A} as the set that contains all possible circuit architectures (or equivalently, the sequences of quantum gates) to build $U(\boldsymbol{\theta})$ in Eqn. (2). Notably, the cardinality of \mathcal{A} is determined by the number of qubits N , the maximum circuit depth L , and the number of allowed types of quantum gates Q , i.e., $|\mathcal{A}| = O(Q^{NL})$. The performance of VQLS heavily depends on the employed circuit architecture $\mathbf{a} \sim \mathcal{A}$, e.g., when \mathbf{a} only includes single qubits gates, the formed $U(\boldsymbol{\theta})$ can never generate entangled states. Suppose that the quantum system noise induced by \mathbf{a} is modeled by the quantum channel $\mathcal{E}_{\mathbf{a}}$. Taking account of the circuit architecture information and the related noise, the objective of VQLS in Eqn. (1) can be rewritten as

$$(\boldsymbol{\theta}^*, \mathbf{a}^*) = \arg \min_{\boldsymbol{\theta} \in \mathcal{C}, \mathbf{a} \in \mathcal{A}} \mathcal{L}(\boldsymbol{\theta}, \mathbf{a}, \mathbf{z}, \mathcal{E}_{\mathbf{a}}). \quad (3)$$

The learning problem formulated in Eqn. (3) implicitly forces the output \mathbf{a}^* as the best quantum circuit architecture to suppress the effect of noise and alleviate the barren plateau influence to attain the best performance. Despite the theoretical feasibility, the optimization of Eqn. (3) is difficult, since the set \mathcal{A} contains exponentially many elements.

The classical analog of the learning problem in Eqn. (3) is the neural network architecture search [27]. Recall that the success of deep learning is largely attributed to the novel neural architectures for specific learning tasks, e.g.,

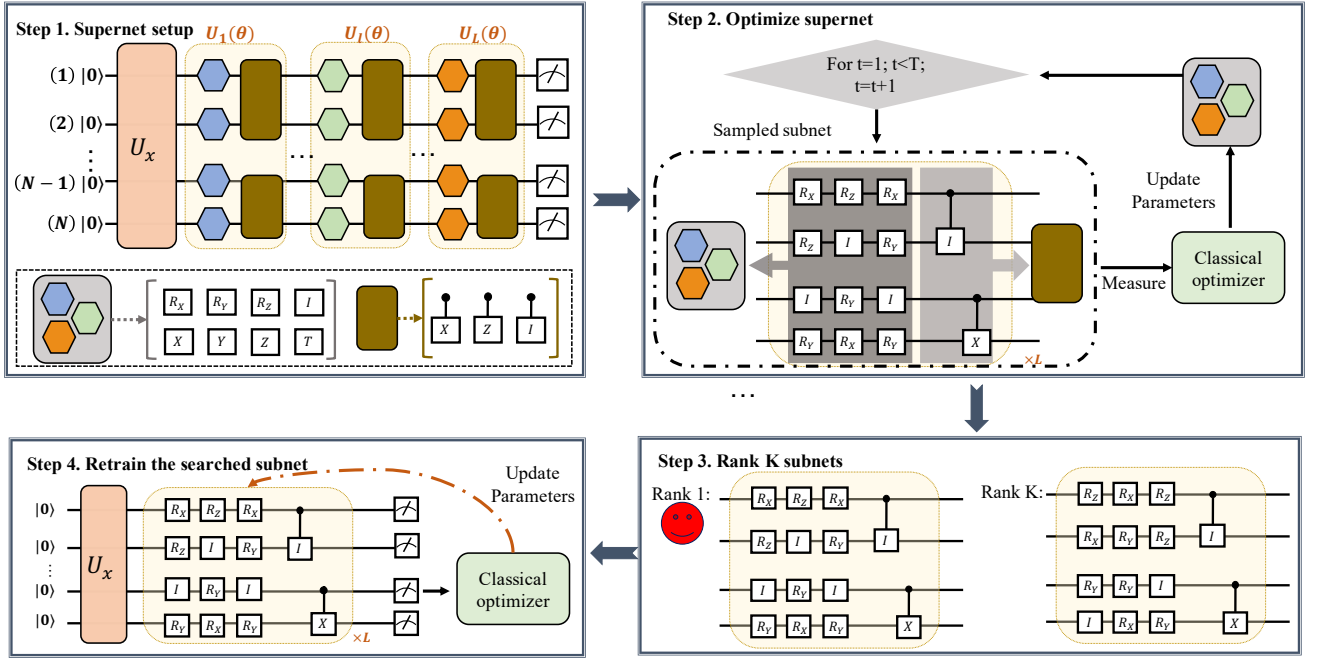


FIG. 1: **The paradigm of quantum architecture search scheme (QAS).** In the Step 1, QAS sets up the supernet \mathcal{A} . The supernet \mathcal{A} collects all possible subnets $\{\mathbf{a}\}$ (i.e., variational quantum circuit architectures), where each \mathbf{a} refers to a specific gates sequence to compose $U(\theta) = \prod_{l=1}^L U_l(\theta)$ in Eqn. (2). For example, one possible subnet \mathbf{a} is that $U_l(\theta)$ for all $l \in [L]$ obeys the same layout and $U_l(\theta) = (\otimes_{i=1}^N R_Z(\theta_i)) (\otimes_{i=1}^N R_Z(\theta_i)) T^{\otimes N}$, where all single qubit gates highlighted by the blue hexagons (the green and orange hexagons) are R_Z gates (R_Y and T gates), and two qubits gates highlighted by the brown rectangle are identities. The supernet \mathcal{A} employs the weight sharing strategy to initialize trainable parameters in all subnets (See Appendix A for details). Specifically, if the layout of single qubit gates to composes $U_l(\theta)$ for any two subnets \mathbf{a} and \mathbf{a}' is identical, then these two subnets share the same training parameters for $U_l(\theta)$. The unitary U_x refers to the encoding layer, e.g., loading classical inputs into the quantum states for machine learning tasks. In the Step 2, given the specified learning task \mathcal{L} , QAS iteratively samples a subnet $\mathbf{a}^{(t)} \in \mathcal{A}$ and optimizes its trainable parameters to minimize \mathcal{L} . After T iterations, QAS moves to the Step 3 and exploits the trained parameters $\theta^{(T)}$ and the predefined \mathcal{L} to compare the performances among K subnets, which are uniformly sampled from \mathcal{A} , and outputs the subnet with the best performance, indicated by the red smiley face. Last, in the Step 4, QAS utilizes the searched subnet and the parameters $\theta^{(T)}$ to retrain the quantum solver with few iterations.

the convolutional neural network for image processing tasks [18], while deep neural networks designed by human experts are generally time-consuming and error-prone [27]. To tackle this issue, neural architecture search approaches, as the process of automating architecture engineering, have been widely explored and achieved state of the art performances in many learning tasks [28–31]. Despite the similar aim, naively generalizing the classical results to the quantum scenario to accomplish Eqn. (3) is infeasible, due to the distinct basic components (i.e., neurons versus quantum gates) and extra limitations in QVLS such as the barren plateau phenomenon, the quantum noise affect, and the physical hardware restrictions. Remarkably, these extra limitations further exacerbate the hardness to search the optimal quantum circuit architecture \mathbf{a}^* compared with the classical setting.

We now elaborate on the implementation of QAS. QAS leverages two key concepts, i.e., the supernet and the weight sharing strategy, which are broadly used in the neural network architecture search [27]. As shown in the Step 1 of Figure 1, the supernet \mathcal{A} , highlighted by hexagons and rectangles, covers all possible subnets (quan-

tum gates sequences) $\{\mathbf{a}\}$ to compose $U(\theta)$ in Eqn. (2). Note that, if the trainable parameters in each subset are initialized independently, the total number of parameters for the supernet is Q_t^{NL} with Q_t being the number of types of trainable gates, e.g., $Q_t = 3$ (i.e., R_X , R_Y , and R_Z) in the Step 1 of Figure 1. Such a parameter space is hard to optimize for the large N and L . To tackle this issue, QAS adopts the weight sharing strategy to initialize the trainable parameters of the supernet. In particular, if the layout of single qubit gates to composes $U_l(\theta)$ for some subnets are identical, then these subnets share the same training parameters for $U_l(\theta)$, no matter how the layout of other layers is varied (See Appendix A for more details). In this way, the number of parameters to be optimized scales with $O(LQ_t^N)$, which is exponentially reduced in terms of L . Once the initialization of the supernet is completed, QAS repeatedly executes the following procedures with T iterations. As exhibited in the Step 2 of Figure 3, at the t -th iteration, QAS uniformly samples a subnet $\mathbf{a}^{(t)} \in \mathcal{A}$ to proceed one optimization step to minimize \mathcal{L} in Eqn. (3), i.e., the parameters in $\mathbf{a}^{(t)}$ is updated to $\theta^{(t+1)} = \theta^{(t)} - \eta \partial \mathcal{L}(\theta^{(t)}, \mathbf{a}^{(t)}, \mathbf{z}, \mathcal{E}_{\mathbf{a}^{(t)}}) / \partial \theta^{(t)}$ with

η being the learning rate. After training, as depicted in the Step 3 of Figure 1, QAS uniformly samples K subnets, ranks their performances, and assigns the subset with the best performance as the output subnet to approximate \mathbf{a}^* . Mathematically, denoted \mathcal{A}_K as the set collecting the sampled K subnets, the output subnet yields

$$\arg \min_{\mathbf{a} \in \mathcal{A}_K} \mathcal{L}(\boldsymbol{\theta}^{(T)}, \mathbf{a}, \mathbf{z}, \mathcal{E}_{\mathbf{a}}). \quad (4)$$

Last, QAS employs the trained parameters $\boldsymbol{\theta}^{(T)}$ to retrain the output subnet, which is shown in Step 4 of Figure 1.

We empirically observe that the competition among different subnets is evidently fierce under the quantum scenario (See Appendix D for details). This phenomenon is contrast with the neural network architecture search. Namely, suppose that the supernet $\mathcal{A} = \mathcal{A}_{\text{good}} \cup \mathcal{A}_{\text{bad}}$ can be decomposed into two subsets, where the subset $\mathcal{A}_{\text{good}}$ (\mathcal{A}_{bad}) collects the subnets such that all of them can attain a relatively good (or bad) performance via independently training, e.g., in the classification task, the subnet in $\mathcal{A}_{\text{good}}$ (\mathcal{A}_{bad}) promises the classification accuracy above (below) 99%. However, when we apply QAS to accomplish the same classification task, some subnets in \mathcal{A}_{bad} may outperform certain subnets in $\mathcal{A}_{\text{good}}$. In other words, adopting a single supernet \mathcal{A} is hard to optimize the trainable parameters of all subnets accurately, so the performances of a portion of subnets in $\mathcal{A}_{\text{good}}$ are worse than independently training.

To relieve the fierce competition among subnets and further boost the performance of QAS, we slightly modify the construction and optimization steps of the supernet. Specifically, instead of exploiting a single supernet to monitor all subnets, we build W supernets $\{\mathcal{A}^{(i)}\}_{i=1}^W$ to optimize W subnets. The parameters among W supernets are optimized independently. In both the training and ranking stages, the sampled subnet $\mathbf{a}^{(t)}$ is fed into W supernets to obtain W values of $\mathcal{L}(\boldsymbol{\theta}^{(T)}, \mathbf{a}^{(t)}, \mathbf{z}, \mathcal{E}_{\mathbf{a}})$, and $\mathbf{a}^{(t)}$ is categorized into the w -th supernet with the minimal \mathcal{L} among all W values. We remark that categorizing of subnets into different supernets has a close relation with the adversarial bandit problems [32]. Moreover, the following theorem shows that the strategy used in QAS outperforms all bandit algorithms in terms of the regret measure.

Theorem 1. *Let W and T be the number of supernets and iterations, respectively. Suppose that the subnet $\mathbf{a}^{(t)}$ is assigned to the $I_w^{(t)}$ -th supernet $\mathcal{A}^{(I_w^{(t)})}$ with $I_w^{(t)} \in [W]$ at the t -th iteration, where the corresponding objective function in Eqn. (3) is $\mathcal{L}(\mathbf{a}^{(t, I_w^{(t)})}) \in [0, 1]$. Define the regret as*

$$R_T = \sum_{t=1}^T \mathcal{L}(\mathbf{a}^{(t, I_w^{(t)})}) - \min_{\{w_t\}_{t=1}^T} \sum_{t=1}^T \mathcal{L}(\mathbf{a}^{(t, w_t)}), \quad (5)$$

where the randomness is over the selection of $I_w^{(t)}$. The method used in QAS to determine $\{I_w^{(t)}\}$ promises the regret $R_T \leq 0$, while the regret for the best bandit algorithms yields $R_T = \Omega(T)$.

We defer the proof of Theorem 1 and the discussion about how to exploit bandit techniques to reduce the runtime to determine $\{I_w^{(t)}\}$ in Appendix B.

We remark that QAS, as a general scheme, can efficiently integrate with other advanced machine learning techniques to further improve its the performance. Concretely, in Appendix C, we elaborate on how to use evolutionary algorithms to advance the ranking state of QAS. Moreover, the searching space covered by supernets of QAS can be effectively adaptive to the physical restrictions, which ensures the compatibility of QAS.

III. Experiment results

The proposed QAS is universal and facilitates a wide range of VQLS based learning tasks, e.g., machine learning [13, 33, 34], quantum chemistry [11, 15], and quantum information processing [35, 36]. In the following, we separately apply QAS to accomplish a classification task and a variational quantum Eigen-solver task to confirm its capability towards the error mitigation and the trainability enhancement. All numerical simulations are implemented in Python in conjunction with the PennyLane package and the Qiskit package [37, 38]. Specifically, PennyLane is the backbone to implement QAS and Qiskit supports different types of noisy models. The Python code related to the examples presented in this study will be available at [39]. Note that our proposal can be easily extended to tackle other VQLS-based learning tasks. We defer the explanation of basic terminologies in machine learning and quantum chemistry (e.g., the epoch number, validation accuracy, the indicator function $\mathbb{1}$, the energy unit Hartree) in Appendix D.

We first apply QAS to achieve a binary classification task under both the noiseless and noisy scenarios. Denote \mathcal{D} as the given dataset, where its construction follows the proposal [13]. The synthetic dataset \mathcal{D} contains $n = 300$ samples. For each example $\{\mathbf{x}^{(i)}, y^{(i)}\}$, the feature dimension of the input $\mathbf{x}^{(i)}$ is three and the corresponding label $y^{(i)} \in \{0, 1\}$ is binary. Some examples of the synthetic dataset \mathcal{D} is shown in Figure 2. At the data preprocessing stage, we split the dataset \mathcal{D} into the training (validation and test) datasets \mathcal{D}_{tr} (\mathcal{D}_{va} and \mathcal{D}_{te}) with size $n_{tr} = 100$ ($n_{va} = 100$ and $n_{te} = 100$). The explicit form of the objective function yields

$$\mathcal{L} = \frac{1}{n_{tr}} \sum_{i=1}^{n_{tr}} (\tilde{y}^{(i)}(\mathcal{A}, \mathbf{x}^{(i)}, \boldsymbol{\theta}) - y^{(i)})^2, \quad (6)$$

where $\{\mathbf{x}^{(i)}, y^{(i)}\} \in \mathcal{D}_{tr}$ and $\tilde{y}^{(i)}(\mathcal{A}, \mathbf{x}^{(i)}, \boldsymbol{\theta}) \in [0, 1]$ is output of quantum classifier as the function of the input $\mathbf{x}^{(i)}$, the supernet \mathcal{A} , and the trainable parameters $\boldsymbol{\theta}$. The training (validation and test) accuracy is measured by $\sum_{i=1}^{n_{tr}} \mathbb{1}_{g(\tilde{y}^{(i)})=y^{(i)}}/n_{tr}$ ($\sum_{i=1}^{n_{va}} \mathbb{1}_{g(\tilde{y}^{(i)})=y^{(i)}}/n_{va}$ and $\sum_{i=1}^{n_{te}} \mathbb{1}_{g(\tilde{y}^{(i)})=y^{(i)}}/n_{te}$) with $g(\tilde{y}^{(i)})$ being the predicted label for $\mathbf{x}^{(i)}$. We also employ the quantum kernel

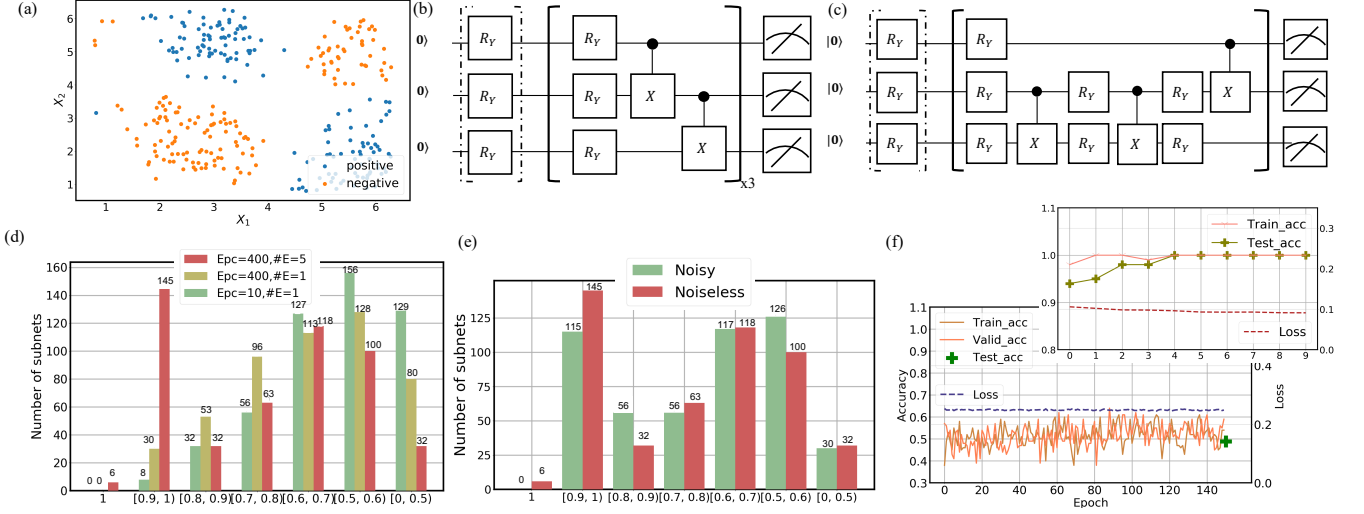


FIG. 2: **Simulation results for the classification task.** (a) The illustration of some examples in \mathcal{D} with first two features. (b) The implementation of the quantum kernel classifier for benchmarking. The quantum gates highlighted by dashed box refer to the encoding layer that transform the classical input $\mathbf{x}^{(i)}$ into the quantum state. The quantum gates located in the solid box refer to $U_l(\boldsymbol{\theta})$ in Eqn. (2) with $L = 3$. (c) The searched subnet of QAS under the noisy setting. (d) The validation performance of QAS under the noiseless case. The label ‘Epc= a , #E= b ’ represents that the number of epochs and supernets is set as $T = a$ and $W = b$, respectively. The x-axis means that the validation accuracy of the sampled subnet is in the range of $[c, d]$, e.g., $c = 0.5$, and $d = 0.6$. (e) The comparison of QAS between the noiseless and noisy cases. The hyper-parameters setting for both cases is $T = 400$, $K = 500$, and $W = 5$. The meaning of x-axis is identical to the subfigure (c). (f) The training performance of the quantum kernel classifier (lower plot) and QAS under the noisy setting (upper plot).

classifier proposed in [13] to benchmark the performance of QAS, where the implementation of such a quantum classifier is shown in Figure 2 (b). See Appendix D for more discussions about the construction of \mathcal{D} and the employed quantum kernel classifier.

The hyper-parameters setting for QAS is as follows. The number of supernets is set as $W = 1$ and $W = 5$, respectively. The circuit depth for all supernets is set as $L = 3$. The number of sampled subnets for ranking, i.e., the Step 3 in Figure 1, is set as $K = 500$. For the single qubit gates, the search space of QAS is fixed to be the rotational quantum gate along Y -axis R_Y . For the two qubits gates, denoted the index of three qubits as $(1, 2, 3)$, QAS explores whether applying CNOT gates to the qubits pair $(1, 2)$, $(1, 3)$, $(2, 3)$ or not. Therefore, the total number of subnets equals to 8^3 .

Under the noiseless setting, the performance of QAS with three different settings is exhibited in Figure 2 (d). In particular, QAS with $W = 1$ and $T = 10$ attains the worst performance, where the validation accuracy for most subnets concentrates on 50% – 60%, highlighted by the green bar. With increasing the number of epochs to $T = 400$ and fixing $W = 1$, the performance is slightly improved, i.e., the number of subnets that achieves validation accuracy above 90% is 30, highlighted by the yellow bar. When $W = 5$ and $T = 400$, the performance of QAS is dramatically enhanced, where the validation accuracy of 151 subnets is above 90%. The comparison between the first two settings indicates the correctness of utilizing QAS to accomplish VQLS based learning tasks in which

QAS learns useful feature information and achieves a better performance with respected to the increased epoch number T . The last two settings reflect the fierce competition phenomenon among subnets and valid the feasibility to adopt W supernets to boost the performance of QAS. We retrain the searched subnet of QAS under the setting $W = 5$ and $T = 400$, both the training and test accuracies converge to 100% within 15 epochs, which is identical to the original quantum kernel classifier (see Appendix D for the omitted simulation results).

The performance of the original quantum kernel classifier is evidently degraded when the depolarizing error for the single qubit gate and two qubits gates are set as 0.05 and 0.2, respectively. As shown in the lower plot of Figure 2 (f), the training and test accuracies of the original quantum kernel classifier drop to 50% (almost conduct a random guess) under the noisy setting. The degraded performance is caused by the accumulated large amount of noise, where the classical optimizer fails to receive the valid optimization information. By contrast, QAS can achieve a good performance under the same noise setting. As shown in Figure 2 (e), with setting $W = 5$ and $T = 400$, the validation accuracy of 115 subnets is above 90% under the noisy setting, while the performance is slightly worse than the noiseless setting. The subnet that attains the highest validation accuracy is shown in 2 (c). Notably, compared with the original quantum kernel classifier in 2 (b), the search subnet contains fewer CNOT gates. This implies that, under the noisy setting formulated above, QAS suppresses the noise

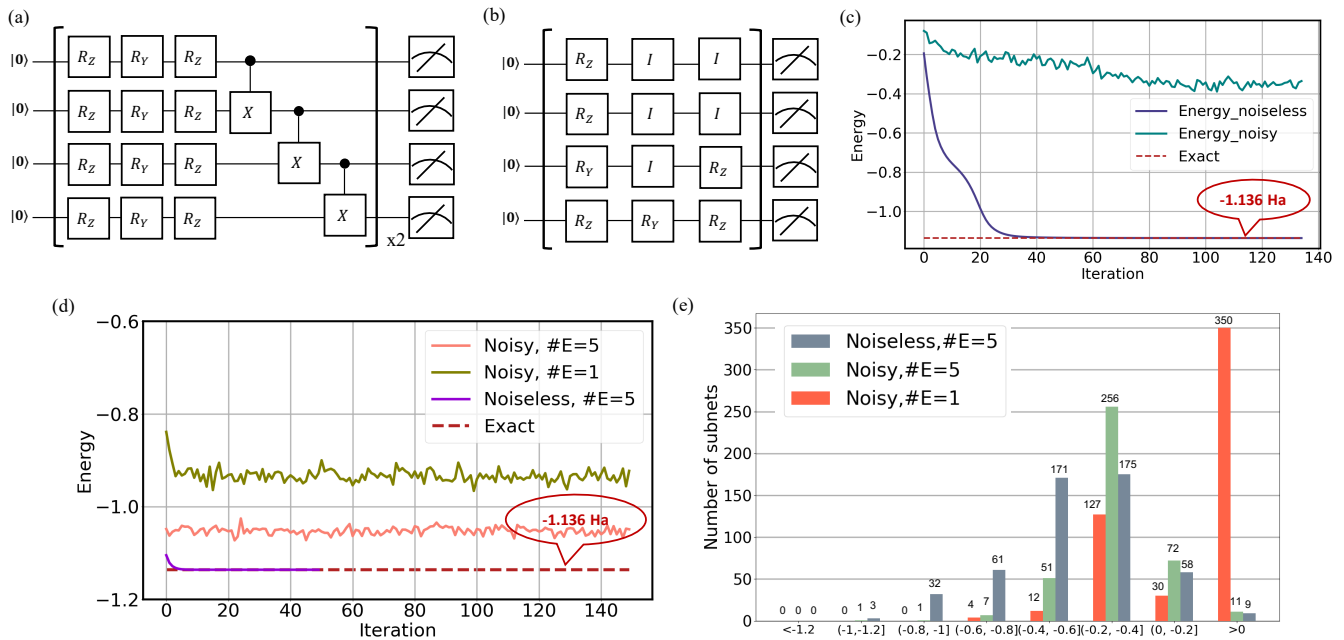


FIG. 3: **Simulation results for the ground state energy estimation of Hydrogen.** (a) The implementation of the conventional variational quantum Eigen-solver (VQE). (b) The searched subnet of QAS under the noisy setting. (c) The training performance of VQE under the noisy and noiseless settings. The label ‘Exact’ refers to the accurate result E_m . (d) The performance of the searched subnet of QAS under both the noisy and noiseless settings. (e) The performance of QAS at the ranking state. The label ‘#E = b’ refers to the number of supernets, i.e., $W = b$. The x-axis means that the estimated energy of the sampled subnet is in the range of $(c, d]$, e.g., $c = -0.6$ Ha, and $d = -0.8$ Ha.

effect and improves the training performance by adopting few CNOT gates. When we retrain the searched subnet with 10 epochs, both the train and test accuracies achieve 100%, as shown in the upper plot of Figure 2 (f).

We next apply QAS to find the ground state energy of the Hydrogen molecule [40, 41] under both the noiseless and noisy scenarios. The molecular hydrogen Hamiltonian can be written as

$$H_h = g + \sum_{i=0}^3 g_i Z_i + \sum_{i=1, k=1, i < k}^3 g_{i,k} Z_i Z_k + g_a Y_0 X_1 X_2 Y_3 + g_b Y_0 Y_1 X_2 X_3 + g_c X_0 X_1 Y_2 Y_3 + g_d X_0 Y_1 Y_2 X_3, \quad (7)$$

where $\{X_i, Z_i, y^{(i)}\}$ denote Pauli matrices acting on the i -th qubit and the real scalars g with or without subscripts are efficiently computable functions of the hydrogen-hydrogen bond length (see Appendix E for details about H_h and g). The ground state energy calculation amounts to compute the lowest energy eigenvalues of H_h , where the accurate value is $E_m = -1.136$ Ha [37]. To tackle this task, the conventional variational quantum Eigen-solver (VQE) [42] optimizes the trainable quantum circuit $U(\theta)$ to prepare the ground state $|\psi^*\rangle = U(\theta^*)|0\rangle^{\otimes 4}$ of H_h , i.e., $E_m = \langle \psi^* | H | \psi^* \rangle$. The implementation of $U(\theta)$ is illustrated in Figure 3 (a). Under the noiseless setting, the estimated energy of VQE fast converges to the target result E_m within 40 iterations, as shown in Figure 3 (c).

The hyper-parameters setting of QAS to compute the lowest energy eigenvalues of H_h is as follows. The number

of supernets is set as $W = 1$ and $W = 5$. The circuit depth for all supernets is $L = 3$. The number of sampled subnets for ranking is $K = 500$. The number of iterations is $T = 500$. For the single qubit gates, the search space of QAS is fixed to be the rotational quantum gates along Y and Z -axis, i.e., R_Y and R_Z . For the two qubits gates, the search space is identical to the classification task. Therefore, the total number of subnets equals to 128^3 . The performance of QAS with $W = 5$ is shown in Figure 3 (d). Specifically, through retraining the searched subnet of QAS with 50 iterations, the estimated energy converges to E_m , which is the same with the conventional VQE.

The performance of the conventional VQE and QAS is distinct when the noisy model described in the classification task is employed. Due to the large amount of gate noise, the estimated ground energy of the conventional VQE converges to -0.4 Ha, as shown in Figure 3 (c). In contrast, the estimated ground energy of QAE with $W = 1$ and $W = 5$ achieves -0.93 Ha and -1.05 Ha, respectively. Both of them are closer to the target result E_m compared with the conventional VQE. Moreover, as shown in Figure 3 (e), more experts imply a better performance of QAE, since the estimated energy of most subnets is below -0.6 Ha when $W = 5$, while the estimated energy of 350 subnets is above 0 Ha when $W = 1$. We illustrate the searched subnet of QAS with $W = 5$ in Figure 3. In particular, to mitigate the affect of gate noise, the searched subnet does not contain any CNOT gates, which are applied to a very large gate noise. Re-

call that a central challenge in quantum computational chemistry is whether NISQ devices can outperform classical methods already available. The achieved results in QAS can provide a good guidance towards this issue. In particular, the searched subnet in Figure 3, which only produces the separable states, suggests that VQE method may not outperform classical methods under the large noise setting formulated above.

We note that more simulation results are given in Appendix E. Furthermore, we implement the conventional VQE and QAS on the real superconducting quantum hardware, i.e., ‘Ibmq_ourense’, to estimate the ground state energy of H_h . Experiment result indicates that the subnet searched by QAS outperforms the conventional VQE, where the estimated energy of the former is -0.81 Ha while the latter is -0.61 Ha.

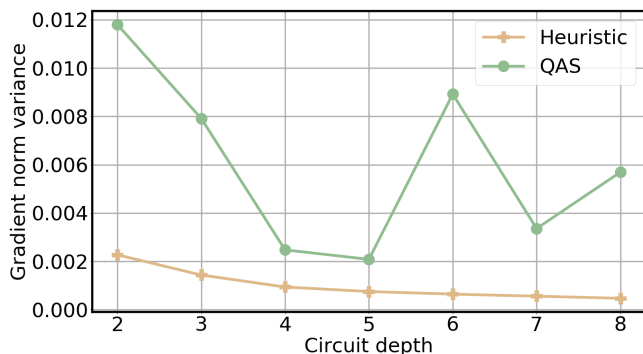


FIG. 4: **The variance of the gradient norm versus the circuit depth.** The label ‘heuristic’ and ‘QAS’ refers to the circuit architecture used in conventional VQE and the subnet searched by QAS, respectively.

We last exhibit how QAS contributes to the alleviation of the barren plateau [22]. Recall one conclusion of the barren plateau is that the gradient vanishes exponentially in the number of layers L . Mathematically, the averaged gradient norm of the objective function in Eqn. (1) will fast converge to zero with respect to L , i.e., $\|\nabla_{\theta}\mathcal{L}(\theta)\|/d \sim O(e^{-L})$. To demonstrate that QAS can alleviate the barren plateau phenomenon, we evaluate the gradient norm of VQE and QAS when they are applied to accomplish the task of finding ground state energy of H_h in Eqn. (7). In particular, we iteratively increase the circuit depth of VQE and QAS from $L = 2$ to $L = 7$, and calculate the variance of the gradient norm $\|\nabla_{\theta}\mathcal{L}(\theta)\|/d$ with respect to the observable Z_0 in H_h , where θ are randomly sampled from the uniform distribution with 2000 times. Note that, for QAS, the circuit architecture for different circuit depths refers to the searched subnet

by optimizing the first non-constant term in H_h . The simulation results under the noiseless setting is shown in Figure 4. As for the conventional VQE, the variance of the gradient norm is continuously decreased when L is increased, which accords with the theoretical results. By contrast, for QAS, the variance of the gradient norm with $L = 8$ is even larger than that of $L = 4$. This result implies that QAS can alleviate the influence of the barren plateau for the large L . Through checking the searched subnet, we observe that QAS is prone to decreasing the usage of CNOT gates to squeeze the circuit depth.

IV. Discussion

In this study, we devise QAS to achieve the error mitigation and trainability enhancement for VQLS-based learning algorithms. Both simulation and experimental results validate the efficiency of QAS. Besides the good performance, QAS is resource and runtime efficient, and is compatible with all quantum systems. To the best of our knowledge, this is the first proposal that can be directly applied to current quantum machines to achieve the error mitigation and the trainability enhancement with scalability. In addition, the incorporation of QAS with other advanced error mitigation techniques and barren plateau alleviation approaches contributes to seek more applications that can be implemented on NISQ machines with potential advantages.

There are many natural questions remaining in the study of QAS. Our future work includes the following three directions. First, we will explore better strategies to sample the subnet at each iteration and more effective methods to allocate the subnet into different supernet. Second, we will design a more advanced weight sharing strategy, which reduces the parameters space of the supernet from $O(LQ_t^N)$ to $O(LQ_tN)$. Last, we aim to leverage some prior information of noisy model to boost the performance of QAS.

Note added:

During the preparation of the manuscript, we notice a relevant paper proposed by Zhang, Hsieh, Zhang, and Hong Yao [43]. In that work the authors also studied an automating quantum circuit architecture engineering strategy. Their proposal can be treated as a classical generalization of the differentiable neural architecture search (DARTS), while the building block of our proposal is one-shot neural architecture search (NAS) [27]. We note that QAS could be more efficient than [43] because the number of subnets that need to be optimized is 1 at each iteration in our work while [43] requires Q_tNL .

[1] Daniel A Lidar and Todd A Brun. *Quantum error correction*. Cambridge university press, 2013.

[2] John Preskill. Quantum computing in the nisq era and beyond. *Quantum*, 2:79, 2018.

- [3] David G Cory, MD Price, W Maas, Emanuel Knill, Raymond Laflamme, Wojciech H Zurek, Timothy F Havel, and Shyamal S Somaroo. Experimental quantum error correction. *Physical Review Letters*, 81(10):2152, 1998.
- [4] Nissim Ofek, Andrei Petrenko, Reinier Heeres, Philip Reinhold, Zaki Leghtas, Brian Vlastakis, Yehan Liu, Luigi Frunzio, SM Girvin, Liang Jiang, et al. Extending the lifetime of a quantum bit with error correction in superconducting circuits. *Nature*, 536(7617):441–445, 2016.
- [5] Christian Kraglund Andersen, Ants Remm, Stefania Lazar, Sebastian Krinner, Nathan Lacroix, Graham J Norris, Mihai Gabureac, Christopher Eichler, and Andreas Wallraff. Repeated quantum error detection in a surface code. *Nature Physics*, pages 1–6, 2020.
- [6] Kristan Temme, Sergey Bravyi, and Jay M Gambetta. Error mitigation for short-depth quantum circuits. *Physical review letters*, 119(18):180509, 2017.
- [7] Ying Li and Simon C Benjamin. Efficient variational quantum simulator incorporating active error minimization. *Physical Review X*, 7(2):021050, 2017.
- [8] Armands Strikis, Dayue Qin, Yanzhu Chen, Simon C Benjamin, and Ying Li. Learning-based quantum error mitigation. *arXiv preprint arXiv:2005.07601*, 2020.
- [9] Piotr Czarnik, Andrew Arrasmith, Patrick J Coles, and Lukasz Cincio. Error mitigation with clifford quantum-circuit data. *arXiv preprint arXiv:2005.10189*, 2020.
- [10] Scott Aaronson and Daniel Gottesman. Improved simulation of stabilizer circuits. *Physical Review A*, 70(5):052328, 2004.
- [11] Alberto Peruzzo, Jarrod McClean, Peter Shadbolt, Man-Hong Yung, Xiao-Qi Zhou, Peter J Love, Alán Aspuru-Guzik, and Jeremy L O’Brien. A variational eigenvalue solver on a photonic quantum processor. *Nature communications*, 5:4213, 2014.
- [12] Edward Farhi and Hartmut Neven. Classification with quantum neural networks on near term processors. *arXiv preprint arXiv:1802.06002*, 2018. URL <https://arxiv.org/abs/1802.06002>.
- [13] Vojtěch Havlíček, Antonio D Córcoles, Kristan Temme, Aram W Harrow, Abhinav Kandala, Jerry M Chow, and Jay M Gambetta. Supervised learning with quantum-enhanced feature spaces. *Nature*, 567(7747):209, 2019.
- [14] Maria Schuld and Nathan Killoran. Quantum machine learning in feature hilbert spaces. *Physical review letters*, 122(4):040504, 2019.
- [15] Frank Carlton Arute, Kunal Arya, Ryan Babbush, Dave Bacon, Joseph Bardin, Rami Barends, Sergio Boixo, Michael Blythe Broughton, Bob Benjamin Buckley, David A Buell, Brian Burkett, Nicholas Bushnell, Yu Chen, Jimmy Chen, Benjamin Chiaro, Roberto Collins, William Courtney, Sean Demura, Andrew Dunsworth, Edward Farhi, Austin Fowler, Brooks Riley Foxen, Craig Michael Gidney, Marissa Giustina, Rob Graff, Steve Habegger, Matthew P Harrigan, Alan Ho, Sabrina Hong, Trent Huang, William J. Huggins, Lev Ioffe, Sergei Isakov, Evan Jeffrey, Zhang Jiang, Cody Jones, Dvir Kafri, Kostyantyn Kechedzhi, Julian Kelly, Seon Kim, Paul Klimov, Alexander Korotkov, Fedor Kostritsa, Dave Landhuis, Pavel Laptev, Mike Lindmark, Erik Lucero, Orion Martin, John Martinis, Jarrod Ryan McClean, Matthew McEwen, Anthony Megrant, Xiao Mi, Masoud Mohseni, Wojtek Mruczkiewicz, Josh Mutus, Ofer Naaman, Matthew Neeley, Charles Neill, Hartmut Neven, Murphy Yuezhen Niu, Thomas E O’Brien, Eric Ostby, Andre Gregory Petukhov, Harry Putterman, Chris Quintana, Pedram Roushan, Nicholas Rubin, Daniel Sank, Kevin Satzinger, Vadim Smelyanskiy, Doug Strain, Kevin Jeffery Sung, Marco Szalay, Tyler Y. Takeshita, Amit Vainsencher, Ted White, Nathan Wiebe, Jamie Yao, Ping Yeh, and Adam Zalcman. Hartree-fock on a superconducting qubit quantum computer. *arXiv:2004.04174*, 2020. URL <https://arxiv.org/abs/2004.04174>.
- [16] Marcello Benedetti, Erika Lloyd, Stefan Sack, and Mattia Fiorentini. Parameterized quantum circuits as machine learning models. *Quantum Science and Technology*, 4(4):043001, 2019.
- [17] Yuxuan Du, Min-Hsiu Hsieh, Tongliang Liu, and Dacheng Tao. Expressive power of parametrized quantum circuits. *Phys. Rev. Research*, 2:033125, Jul 2020. doi: 10.1103/PhysRevResearch.2.033125. URL <https://link.aps.org/doi/10.1103/PhysRevResearch.2.033125>.
- [18] Ian Goodfellow, Yoshua Bengio, and Aaron Courville. *Deep learning*. MIT press, 2016.
- [19] Yuxuan Du, Min-Hsiu Hsieh, Tongliang Liu, Dacheng Tao, and Nana Liu. Quantum noise protects quantum classifiers against adversaries. *arXiv preprint arXiv:2003.09416*, 2020.
- [20] Caglar Gulcehre, Marcin Moczulski, Misha Denil, and Yoshua Bengio. Noisy activation functions. In *International conference on machine learning*, pages 3059–3068, 2016.
- [21] Stephan Zheng, Yang Song, Thomas Leung, and Ian Goodfellow. Improving the robustness of deep neural networks via stability training. In *Proceedings of the IEEE conference on computer vision and pattern recognition*, pages 4480–4488, 2016.
- [22] Jarrod R McClean, Sergio Boixo, Vadim N Smelyanskiy, Ryan Babbush, and Hartmut Neven. Barren plateaus in quantum neural network training landscapes. *Nature communications*, 9(1):1–6, 2018.
- [23] Samson Wang, Enrico Fontana, Marco Cerezo, Kunal Sharma, Akira Sone, Lukasz Cincio, and Patrick J Coles. Noise-induced barren plateaus in variational quantum algorithms. *arXiv preprint arXiv:2007.14384*, 2020.
- [24] Yuxuan Du, Min-Hsiu Hsieh, Tongliang Liu, Shan You, and Dacheng Tao. On the learnability of quantum neural networks. *arXiv preprint arXiv:2007.12369*, 2020.
- [25] Kevin J. Sung, Matthew P. Harrigan, Nicholas C. Rubin, Zhang Jiang, Ryan Babbush, and Jarrod R. McClean. An exploration of practical optimizers for variational quantum algorithms on superconducting qubit processors, 2020.
- [26] M Cerezo, Akira Sone, Tyler Volkoff, Lukasz Cincio, and Patrick J Coles. Cost-function-dependent barren plateaus in shallow quantum neural networks. *arXiv preprint arXiv:2001.00550*, 2020.
- [27] Thomas Elsken, Jan Hendrik Metzen, and Frank Hutter. Neural architecture search: A survey. *Journal of Machine Learning Research*, 20:1–21, 2019.
- [28] Hieu Pham, Melody Guan, Barret Zoph, Quoc Le, and Jeff Dean. Efficient neural architecture search via parameters sharing. In *International Conference on Machine Learning*, pages 4095–4104, 2018.
- [29] Chenxi Liu, Barret Zoph, Maxim Neumann, Jonathon Shlens, Wei Hua, Li-Jia Li, Li Fei-Fei, Alan Yuille, Jonathan Huang, and Kevin Murphy. Progressive neural architecture search. In *Proceedings of the European Conference on Computer Vision (ECCV)*, pages 19–34, 2018.

- [30] Shan You, Tao Huang, Mingmin Yang, Fei Wang, Chen Qian, and Changshui Zhang. Greedynas: Towards fast one-shot nas with greedy supernet. In *Proceedings of the IEEE/CVF Conference on Computer Vision and Pattern Recognition*, pages 1999–2008, 2020.
- [31] Yibo Yang, Hongyang Li, Shan You, Fei Wang, Chen Qian, and Zhouchen Lin. Ista-nas: Efficient and consistent neural architecture search by sparse coding. *arXiv preprint arXiv:2010.06176*, 2020.
- [32] Sébastien Bubeck and Nicolo Cesa-Bianchi. Regret analysis of stochastic and nonstochastic multi-armed bandit problems. *arXiv preprint arXiv:1204.5721*, 2012.
- [33] Yuxuan Du, Min-Hsiu Hsieh, Tongliang Liu, and Dacheng Tao. Implementable quantum classifier for nonlinear data. *arXiv preprint arXiv:1809.06056*, 2018.
- [34] Iris Cong, Soonwon Choi, and Mikhail D Lukin. Quantum convolutional neural networks. *Nature Physics*, 15(12):1273–1278, 2019.
- [35] Ryan LaRose, Arkin Tikku, Étude O’Neel-Judy, Lukasz Cincio, and Patrick J Coles. Variational quantum state diagonalization. *npj Quantum Information*, 5(1):1–10, 2019.
- [36] Yuxuan Du, Min-Hsiu Hsieh, and Dacheng Tao. Efficient online quantum generative adversarial learning algorithms with applications. *arXiv preprint arXiv:1904.09602*, 2019.
- [37] Ville Bergholm, Josh Izaac, Maria Schuld, Christian Gogolin, Carsten Blank, Keri McKiernan, and Nathan Killoran. PennyLane: Automatic differentiation of hybrid quantum-classical computations. *arXiv preprint arXiv:1811.04968*, 2018.
- [38] Qiskit: An open-source framework for quantum computing, 2019.
- [39] https://github.com/yuxuan-du/Quantum_architecture_search/.
- [40] Peter JJ O’Malley, Ryan Babbush, Ian D Kivlichan, Jonathan Romero, Jarrod R McClean, Rami Barends, Julian Kelly, Pedram Roushan, Andrew Tranter, Nan Ding, et al. Scalable quantum simulation of molecular energies. *Physical Review X*, 6(3):031007, 2016.
- [41] Abhinav Kandala, Antonio Mezzacapo, Kristan Temme, Maika Takita, Markus Brink, Jerry M Chow, and Jay M Gambetta. Hardware-efficient variational quantum eigensolver for small molecules and quantum magnets. *Nature*, 549(7671):242–246, 2017.
- [42] Giuseppe Davide Paparo, Vedran Dunjko, Adi Makmal, Miguel Angel Martin-Delgado, and Hans J Briegel. Quantum speedup for active learning agents. *Physical Review X*, 4(3):031002, 2014.
- [43] Shi-Xin Zhang, Chang-Yu Hsieh, Shengyu Zhang, and Hong Yao. Differentiable quantum architecture search, 2020.
- [44] Zichao Guo, Xiangyu Zhang, Haoyuan Mu, Wen Heng, Zechun Liu, Yichen Wei, and Jian Sun. Single path one-shot neural architecture search with uniform sampling. In *Computer Vision – ECCV 2020*, pages 544–560, Cham, 2020. Springer International Publishing. ISBN 978-3-030-58517-4.
- [45] Sébastien Gerchinovitz and Tor Lattimore. Refined lower bounds for adversarial bandits. In *Advances in Neural Information Processing Systems*, pages 1198–1206, 2016.
- [46] Kalyanmoy Deb, Amrit Pratap, Sameer Agarwal, and TAMT Meyarivan. A fast and elitist multiobjective genetic algorithm: Nsga-ii. *IEEE transactions on evolutionary computation*, 6(2):182–197, 2002.
- [47] Richard S Sutton et al. *Introduction to reinforcement learning*, volume 135.
- [48] W Pirie. Spearman rank correlation coefficient. *Encyclopedia of statistical sciences*, 12, 2004.
- [49] M. G. Kendall. A new measure of rank correlation. *Biometrika*, 30(1/2):81–93, 1938.
- [50] Sam McArdle, Suguru Endo, Alan Aspuru-Guzik, Simon C Benjamin, and Xiao Yuan. Quantum computational chemistry. *Reviews of Modern Physics*, 92(1):015003, 2020.
- [51] James Stokes, Josh Izaac, Nathan Killoran, and Giuseppe Carleo. Quantum natural gradient. *Quantum*, 4:269, 2020.

We organize the appendix as follows. In Appendix A, we elaborate on the implementation of the supernet and the weight sharing strategy. In Appendix B, we establish the connection between the bandit learning and the subnet assignment task, provide the proof of Theorem 1, and discuss how to exploit bandit learning algorithms to advance the subnet assignment task. Afterwards, we exhibit how to employ evolutionary algorithms to advance the ranking stage of QAS in Appendix C. We then provide explanations and simulation results related to the classification task in Appendix D. We last present more details about the quantum chemistry tasks in Appendix E.

A. Supernet and the weight sharing strategy

Here we elaborate on the weight sharing strategy used in QAS. Recall the aim of the weight sharing strategy. Denote the number of qubits as N and the maximum layer number of $U(\theta)$ in Eqn. (2) as L . Suppose that the allowed operations for the single qubit gate are $\{R_X, R_Y, R_Z\}$. As for the two qubits gates, the allowed operation is applying CNOT gate to any two qubits or do nothing. Then, the supernet contains in total $(3^N \cdot 2^{(C_N^2)})^L$ subnets, where for each layer $U_l(\theta)$ the number of gates sequence is $3^N \cdot 2^{(C_N^2)}$. To reduce the parameter space of supernet, QAS adopts the weight sharing strategy. Namely, for all subnets, once the sequence of single qubit gates in $U_l(\theta)$ is identical, they share the same parameters at the l -th layer. A concrete example is shown in Figure 5. Specifically, the single qubit gate sequence of $U_l(\theta)$ for the left and middle circuits (subnets) is identical, which is in the order $[R_Y(\theta_{l,1}), R_Z(\theta_{l,2}), R_Y(\theta_{l,3}), R_Y(\theta_{l,4})]$. Then the trainable parameters $\{\theta_{l,i}\}_{i=1}^4$ used in these two circuits are always same, no matter how the connection of CNOT gates is varied. By contrast, although the middle and right circuits have the same CNOT gates arrangements in $U_l(\theta)$, these two circuits cannot share the parameters in the l -th layer, since the single qubit gates sequence in the right circuit is in the order $[R_Y(\theta'_{l,1}), R_Y(\theta'_{l,2}), R_Y(\theta'_{l,3}), R_Y(\theta'_{l,4})]$.

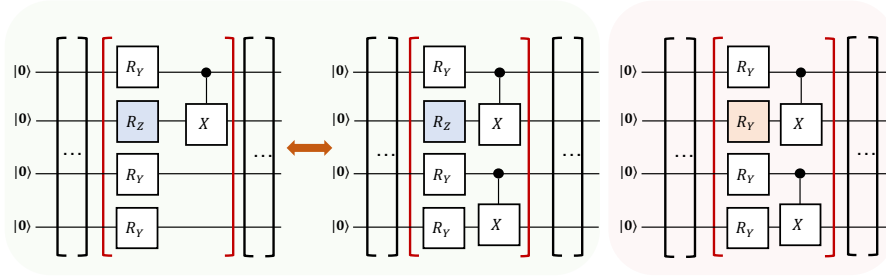


FIG. 5: **The weight sharing strategy.** The red box for all three plots refers to the sampled quantum gates sequence in $U_l(\theta)$, while the black boxes represent other trainable unitary layers $\{U_j(\theta)\}$ with $j \neq l$. The $U_l(\theta)$ in the left and middle circuits, highlighted by the green region, share the same training parameters. The $U_l(\theta)$ right circuit, highlighted by the red region, does not share the parameters with other two quantum circuits.

B. The subset assignment task

In this section, we first connect the subnet assignment task with the adversarial bandit learning problem. We then provide the proof of Theorem 1. We last explain how to employ advanced bandit learning algorithms to reduce the runtime to assign the given subnet.

1. The connection between the adversarial bandit learning and the subnet assignment

In the adversarial bandit learning [32], a player has W possible arms to choose. Denote the total number of iterations as T . At the t -th iteration,

- The player chooses an arm $w^{(t)} \in [W]$ with a deterministic strategy or sampled from a certain distribution \mathcal{P}_w ;
- Adversary chooses action $z^{(t)}(w^{(t)})$ for the chosen arm;
- The cost of the selected arm $w^{(t)}$, i.e., $c(w^{(t)}) : w^{(t)} \in [W]$, is revealed.

The goal of the adversarial bandit learning is minimizing the total cost over the T iterations. The performance of the bandit algorithm is quantified by the regret r_T , i.e.,

$$r_T = \sum_{t=1}^T c(w^{(t)}, z^{(t)}) - \min_{w \in [W]} \sum_{t=1}^T c(w, z^{(t)}). \quad (\text{B1})$$

Intuitively, the regret r_T compares the the cumulative cost of the selected arms $\{w^{(t)}\}_{t=1}^T$ with the best arm in hindsight. If $r_T = o(T)$, where the regret can be either negative or scales at most sublinearly with T , we say that the player is learning; Otherwise, when $r_T = \Theta(T)$ such that the regret scales linearly with T , we say that the player the averaged cost per-iteration does not decrease with time.

We now utilize the language of the adversarial bandit learning to restate the subnet assignment problem. In QAS, each arm refers to a supernet and the number of arms equals to the number of employed supernets. The action $z^{(t)}$ selected by the adversary corresponds to the subnet $\mathbf{a}^{(t)} \in \mathcal{A}$. The cost c is equivalent to the objection function $\mathcal{L}(\boldsymbol{\theta}^{(t)}, \mathbf{a}^{(t,w)})$ defined in Eqn. (3). The goal of the subnet assignment is to allocate $\mathbf{a}^{(t)}$ to the best sequence of arms (supernets) $\{I_w^{(t)}\}_{t=1}^T$ to minimize the cumulative cost, where the regret defined in Eqn. (B1) can be rewritten as

$$\tilde{R}_T = \sum_{t=1}^T \mathcal{L}(\boldsymbol{\theta}^{(t)}, \mathbf{a}^{(t, I_w^{(t)})}) - \min_{w \in [W]} \sum_{t=1}^T \mathcal{L}(\boldsymbol{\theta}^{(t)}, \mathbf{a}^{(t,w)}). \quad (\text{B2})$$

2. Proof of Theorem 1

The proof of Theorem 1 exploits the following lemma.

Lemma 1 (Theorem1, [45]). *Suppose $W \geq 2$ and $\delta \in (0, 1/4)$ and $T \geq 32(K-1) \log(2/\delta)$, then there exists a sequence of subnets, or equivalently, the losses $\{\mathcal{L}(\boldsymbol{\theta}^{(t)}, \mathbf{a}^{(t, w_t)})\}_{t=1}^T$ such that the regret in Eqn. (B2) follows*

$$\mathcal{P} \left(\tilde{R}_T \geq \frac{1}{27} \sqrt{(K-1)T \log(1/(4\delta))} \right) \geq \delta/2. \quad (\text{B3})$$

The lower bound in Lemma 1 indicates that under the adversarial setting, there does not exist a bandit algorithm can achieve the smaller regret than $\Omega(\sqrt{KT \log(1/\delta)})$ with probability at least $1 - \delta$.

We are now ready to prove Theorem 1.

Proof of Theorem 1. Here we first prove the regret R_T in Eqn. (5) for the strategy used in QAS. We then quantify the lower bound of R_T for all bandit algorithms.

Recall the assignment strategy used in QAS. Given the sampled subnet $\mathbf{a}^{(t)}$, QAS feeds this subnet into W supernets and compares W values of objective functions, i.e., $\{\mathcal{L}(\boldsymbol{\theta}^{(t)}, \mathbf{a}^{(t,w)})\}_{w=1}^W$. Then, the subnet $\mathbf{a}^{(t)}$ is assigned to the $I_w^{(t)}$ -th supernet as

$$I_w^{(t)} = \arg \min_{w=1, \dots, W} \mathcal{L}(\boldsymbol{\theta}^{(t)}, \mathbf{a}^{(t,w)}). \quad (\text{B4})$$

By exploiting the explicit definition of $I_w^{(t)}$ in Eqn. (B4), the regret R_T in Eqn. (5) yields

$$\begin{aligned} R_T &= \sum_{t=1}^T \mathcal{L}(\boldsymbol{\theta}^{(t)}, \mathbf{a}^{(t, I_w^{(t)})}) - \min_{\{w_t\}_{t=1}^T} \sum_{t=1}^T \mathcal{L}(\boldsymbol{\theta}^{(t)}, \mathbf{a}^{(t, w_t)}) \\ &= \sum_{t=1}^T \min_{w=1, \dots, W} \mathcal{L}(\boldsymbol{\theta}^{(t)}, \mathbf{a}^{(t,w)}) - \min_{\{w_t\}_{t=1}^T} \sum_{t=1}^T \mathcal{L}(\boldsymbol{\theta}^{(t)}, \mathbf{a}^{(t, w_t)}) \\ &\leq 0, \end{aligned} \quad (\text{B5})$$

where the equality happens in the last equality when $\min_w \mathcal{L}(\boldsymbol{\theta}^{(t)} \mathbf{a}^{(t,w)}) = \min_{w'} \mathcal{L}(\boldsymbol{\theta}^{(t)} \mathbf{a}^{(t,w')})$ for all $w, w' \in [W]$.

We next prove that the regret of all bandit algorithm is lower bounded by $\Omega(\sqrt{WT})$. The discrepancy between the regret R_T in Eqn. (5) and \tilde{R}_T in Eqn. (B2) yields

$$\begin{aligned} R_T - \tilde{R}_T &= \left(\sum_{t=1}^T \mathcal{L}(\boldsymbol{\theta}^{(t)}, \mathbf{a}^{(t, I_w^{(t)})}) - \min_{\{w_t\}_{t=1}^T} \sum_{t=1}^T \mathcal{L}(\boldsymbol{\theta}^{(t)}, \mathbf{a}^{(t, w_t)}) \right) - \left(\sum_{t=1}^T \mathcal{L}(\boldsymbol{\theta}^{(t)}, \mathbf{a}^{(t, I_w^{(t)})}) - \min_{w \in [W]} \sum_{t=1}^T \mathcal{L}(\boldsymbol{\theta}^{(t)}, \mathbf{a}^{(t, w)}) \right) \\ &= \min_{w \in [W]} \sum_{t=1}^T \mathcal{L}(\boldsymbol{\theta}^{(t)}, \mathbf{a}^{(t, w)}) - \min_{\{w_t\}_{t=1}^T} \sum_{t=1}^T \mathcal{L}(\boldsymbol{\theta}^{(t)}, \mathbf{a}^{(t, w_t)}) \\ &\geq 0, \end{aligned} \tag{B6}$$

where the equality happens when $\min_{w_t} \mathcal{L}(\boldsymbol{\theta}^{(t)}, \mathbf{a}^{(t, w_t)}) = \min_{w_{t'}} \mathcal{L}(\boldsymbol{\theta}^{(t')}, \mathbf{a}^{(t', w_{t'})})$ for all $t, t' \in [T]$.

In conjunction with Eqn. (B6) and Lemma 1, we achieve

$$\mathcal{P} \left(R_T \geq \frac{1}{27} \sqrt{(K-1)T \log(1/(4\delta))} \right) \geq \delta/2. \tag{B7}$$

In other words, for the subset assignment task, there does not exist a bandit algorithm can achieve $R_T \leq \Omega(\sqrt{KT \log(1/\delta)})$ with probability at least $1 - \delta$.

Based on Eqn. (B6) and Eqn. (B7), we conclude that that no bandit learning algorithm can achieved a lower regret bound than that of the strategy adopted in QAS. \square

3. Applying bandit learning algorithms to the subnet assignment

Here we discuss how to apply bandit learning algorithms to benefit the subnet assignment task, especially for the runtime cost. Recall the strategy used in QAS for the subnet assignment. At each iteration, the sampled subnet should feed into W supernet separately and then compare the returned W loss values. The runtime complexity becomes expensive for a large W . The adversarial bandit learning algorithms is a promising solution to tackle the runtime issue. As explained in Appendix B 1, the subnet is only required to feed into one supernet at each iteration, while the price is inducing a large regret bound.

Algorithm 1 Evolutionary subnets sampling in the ranking stage

Require: Supernet \mathcal{A} , population size N_{pop} , number of generations G_T , the input data \mathbf{z} , the predefined objective function \mathcal{L} .
Random initialize population P_0 and set $E = \emptyset$; # evaluation set E which stores all evaluated subntes with corresponding scores
for $i = 0, 1, \dots, G_T - 1$ **do**
 $Q_i = \text{make-new-pop}(P_i)$;
 # generate offspring population Q_i using binary tournament selection, recombination, and mutation operators
 $R_i = P_i \cup Q_i$;
 $F_i = \text{fast-non-dominated-sort}(R_i)$; # generate all nondominated fronts of R_i
 $P_{i+1} = \emptyset$ and $j = 0$;
 while $|P_{i+1}| + |F_i| \leq N_{pop}$ **do**
 $\text{crowding-distance-assignment}(F_i)$; # calculate crowding-distance in F_j
 $P_{i+1} = P_{i+1} \cup F_j$;
 $j = j + 1$;
 end while
 $E_i = \text{evaluation-architectures}(F_j, \mathbf{z}, \mathcal{L})$; # evaluate subnets with validation data \mathcal{D}_{va}
 $E = E \cup E_i$; # extend E_i to E ;
 $\text{Sort}(F_j, E_i)$; # sort in descending order using E_i
 $P_{i+1} = P_{i+1} \cup F_j[1 : (N_{pop} - |P_{i+1}|)]$; # choose the first $(N_{pop} - |P_{i+1}|)$ elements of F_j
end for
return Subnet with the highest score in E

C. Improving the ranking stage of QAS

Recall the approach adopted in the step 3 in Figure 1 of QAS is uniformly sampling K subnets from the supernet \mathcal{A} . The aim of step is sampling some good subnets from $\mathcal{A}_{\text{good}}$ and selecting the one with the top performance. However, the uniformly sampling method implies the sampled subnets may be come from \mathcal{A}_{bad} with a certain high probability.

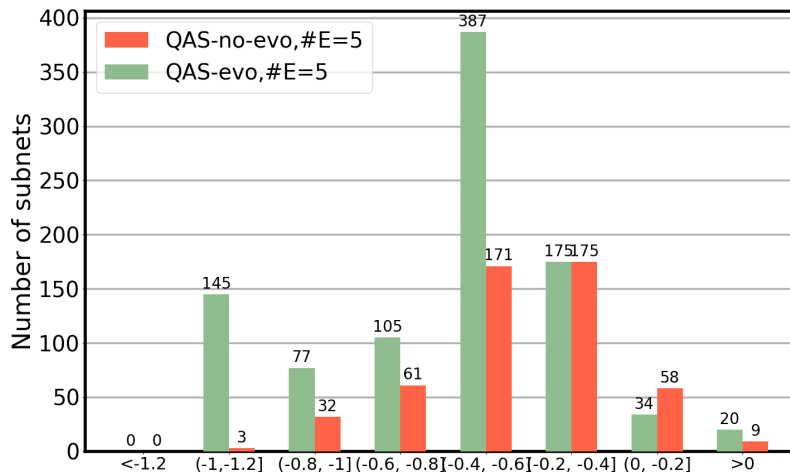


FIG. 6: **Simulation result of QAS with the evolutionary assisted ranking algorithm.** The label ‘QAS-no-evo, # E=5’ and ‘QAS-evo, # E=5’ refer to the QAS introduced in the main text and QAS assisted by evolutionary algorithm with the number of supernets being $W = 5$, respectively. The x-axis refers to the estimated energy of the given subnet is in the range of $(a \text{ Ha}, b \text{ Ha}]$ with $a, b \in \mathbb{R}$.

Here we utilize evolutionary algorithms to tackle this issue. Algorithm 1 summarizes how to apply the evolutionary algorithm —nondominated sorting genetic algorithm II (NSGA-II) [46], to accomplish the subnet ranking problem. The intuition behind Algorithm 1 is actively searching the potential subnet with good performance instead of uniformly sampling a subnet from all possible circuit architectures.

We apply QAS with the evolutionary algorithm in Algorithm 1 to tackle the ground state energy estimation problem described in the main text. Note that all hyper-parameters settings are identical to the uniformly sampling case, except for the settings related to the evolutionary algorithm. Particularly, we set the population size as $N_{pop} = 50$ and the number of generations as $G_T = 20$. The simulation results under the noiseless setting are shown in Figure 6. In particular, QAS assisted by Algorithm 1 searches in total 943 subnets, and the estimated energy of 143 subnets (15.2%) lies in the range from -1 Ha to -1.2 Ha . By contrast, QAS with uniformly sampling strategy only finds 3 subnets among in total 500 subnets (0.6%) in the same range. This result empirically confirms that evolutionary algorithms can advance the performance of QAS.

We remark that other advanced machine learning techniques such as reinforcement learning [47] can also be exploited to benefit the performance of QAS.

D. The synthetic dataset classification task

In this section, we first introduce some basic terminologies in machine learning to make our description self-consistent in Appendix D 1. We then explain how to construct the synthetic dataset \mathcal{D} in Appendix D 2. We last provide the simulation results omitted in the main text, especially for the fierce competition phenomenon, in Appendix D 3.

1. Basic terminologies in machine learning

When we apply QAS to accomplish the classification task, the terminology epoch, which is broadly used in the field of machine learning [18], is employed to replace the iteration. Intuitively, an epoch means that an entire dataset is passed forward through the quantum learning model. For the quantum kernel classifier used in the main text, each training example in \mathcal{D}_{tr} is fed into the quantum circuit in sequence to acquire the predicted label. Since \mathcal{D}_{tr} includes in total 100 examples, it will take 100 iterations to complete 1 epoch.

In the synthetic classification task, we split the datasets into the three parts, i.e., the training, validation, and test datasets, following the convention of machine learning [18]. The training dataset \mathcal{D}_{tr} is used to optimize the trainable parameters during the learning process. The function of the validation dataset \mathcal{D}_{va} is estimating how well the classifier has been trained. During T epochs, the learner records the trainable parameters that achieves to the highest validation

accuracy as the output of training parameters. Mathematically, the output parameters satisfy

$$\hat{\boldsymbol{\theta}} = \max_{\{\boldsymbol{\theta}^{(t)}\}_{t=1}^T} \sum_i \mathbb{1}_{\tilde{y}^{(i)}(\boldsymbol{\theta}^{(t)}, \mathbf{x}^{(i)})=y^{(i)}}, \quad (\text{D1})$$

where $\{\mathbf{x}^{(i)}, y^{(i)}\} \in \mathcal{D}_{va}$, $\tilde{y}^{(i)}$ is the prediction of the classifier given $\tilde{y}^{(i)}$ and $\mathbf{x}^{(i)}$, and $\mathbb{1}_z$ is the indicator function that takes the value 1 if the condition z is satisfied and zero otherwise. Finally, the output parameters $\hat{\boldsymbol{\theta}}$ are applied to the test dataset to benchmark the performance of the trained classifier.

2. Implementation of the synthetic dataset

Here we recap the method to construct of the synthetic dataset proposed in [13]. Denote the encoding layer as

$$U_{\mathbf{x}} = R_Y(\mathbf{x}_1) \otimes R_Y(\mathbf{x}_2) \otimes R_Y(\mathbf{x}_3). \quad (\text{D2})$$

Let the optimal trainable circuit be

$$U^*(\boldsymbol{\theta}^*) = \prod_{l=1}^3 U_l^*(\boldsymbol{\theta}_l^*), \quad (\text{D3})$$

where $U_l^*(\boldsymbol{\theta}_l^*) = \otimes_{j=1}^3 R_Y(\boldsymbol{\theta}_{l,j}^*)(\text{CNOT} \otimes I_2)(I_2 \otimes \text{CNOT})$ and the parameters $\boldsymbol{\theta}^*$ is uniformly sampled from $[0, 2\pi)^9$. To establish the synthetic \mathcal{D} used in the main text, we encode a data point $\mathbf{x}^{(i)}$ that is uniformly sampled from $(0, 1)^3$ into $U_{\mathbf{x}^{(i)}}$ followed by $U(\boldsymbol{\theta}^*)$, and then measure the generated state by the operator $\Pi = \mathbb{I}_4 \otimes |0\rangle\langle 0|$. The data point is labeled as $y^{(i)} = 1$ if

$$\langle 000|U_{\mathbf{x}^{(i)}}^\dagger U^*(\boldsymbol{\theta}^*)\Pi U^*(\boldsymbol{\theta}^*)U_{\mathbf{x}^{(i)}}|000\rangle \geq 0.75. \quad (\text{D4})$$

The label of $\mathbf{x}^{(i)}$ is assigned as $y^{(i)} = 0$ if

$$\langle 000|U_{\mathbf{x}^{(i)}}^\dagger U^*(\boldsymbol{\theta}^*)\Pi U^*(\boldsymbol{\theta}^*)U_{\mathbf{x}^{(i)}}|000\rangle \leq 0.25. \quad (\text{D5})$$

Note that, if the measured result is in the range $(0.25, 0.75)$, we drop this data point and sample a new one. By repeating the above procedure, we can built the synthetic dataset \mathcal{D} .

3. More results about the synthetic dataset classification

Here we first introduce how to use the quantum classifier to conduct the prediction. Recall that given the data point $\mathbf{x}^{(i)} \in \mathcal{D}$ at the t -th epoch, the quantum classifier is composed of two unitaries, i.e., $U_{\mathbf{x}^{(i)}}$ and $U(\boldsymbol{\theta}^{(t)})$. The quantum gates sequence in $U(\boldsymbol{\theta}^{(t)})$ is fixed for the conventional quantum kernel classifier as shown in Figure 2 (b), while the arrangement of quantum gates for QAS depends on the sampled subnet. The output of the data point $\mathbf{x}^{(i)} \in \mathcal{D}$ in Eqn. (6) yields

$$\tilde{y}(\mathcal{A}, \mathbf{x}^{(i)}, \boldsymbol{\theta}^{(t)}) = \langle 000|U_{\mathbf{x}^{(i)}}^\dagger U(\boldsymbol{\theta}^{(t)})\Pi U(\boldsymbol{\theta}^{(t)})U_{\mathbf{x}^{(i)}}|000\rangle. \quad (\text{D6})$$

For the conventional classifier, we have

$$\tilde{y}(\mathbf{x}^{(i)}, \boldsymbol{\theta}^{(t)}) = \langle 000|U_{\mathbf{x}^{(i)}}^\dagger U(\boldsymbol{\theta}^{(t)})\Pi U(\boldsymbol{\theta}^{(t)})U_{\mathbf{x}^{(i)}}|000\rangle. \quad (\text{D7})$$

The predicted label for $\mathbf{x}^{(i)}$ in Eqn. (6) is defined as

$$g(\tilde{y}(\mathbf{x}^{(i)}, \boldsymbol{\theta}^{(t)})) = \begin{cases} 0, & \text{if } \tilde{y}(\mathbf{x}^{(i)}, \boldsymbol{\theta}^{(t)}) < 0.5 \\ 1, & \text{otherwise} \end{cases}. \quad (\text{D8})$$

We then provide the simulation results of the conventional quantum kernel classifier and QAS towards the synthetic dataset \mathcal{D} under the noiseless setting. As exhibited in Figure 7 (a), both the training and validation accuracies of the conventional quantum kernel classifier fast converge to 100% after 80 epochs. The test accuracy also reaches 100%,

highlighted by the green marker. Meanwhile, the loss \mathcal{L} decreases to 0.24. These results indicate that the conventional quantum kernel classifier with the protocol as depicted in Figure 2 (b) can well learn the synthetic dataset \mathcal{D} . The training procedure of QAS under the noiseless setting is identical to the noisy setting as formulated in the main text. Specifically, we set $T = 400$ and $W = 1$ in the training stage (the step 2), $K = 500$ in the ranking stage (the step 3), and $T = 10$ in the retraining stage (the step 4). Figure 7 (c) demonstrates the searched subnet in the step 3. Compared to the conventional quantum kernel classifier, the searched subnet includes fewer CNOT gates, which is more reconcile for the physical implementation. Figure 7 (b) illustrates the learning performance of the searched subnet. Namely, both the training and test accuracies converge to 100% after one epoch. These results reflect that QAS can well learn the synthetic dataset \mathcal{D} under the noiseless setting. Note that for all simulation results related to classification tasks, the Adam optimizer [18] is exploited to update the training parameters of the quantum kernel classifier and QAS. The learning rate is set as 0.05.

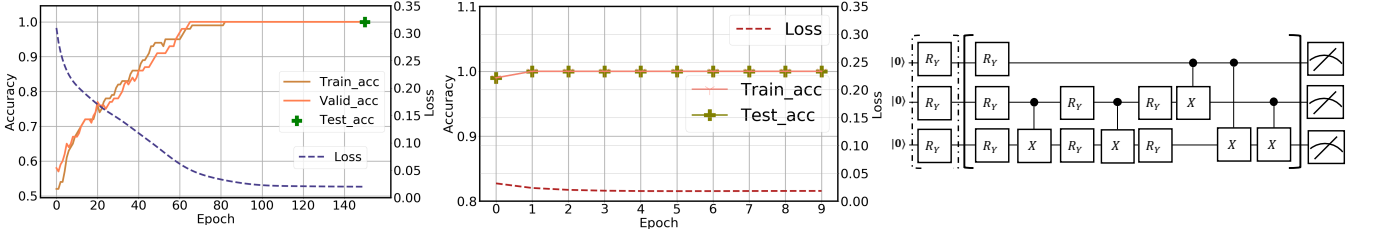


FIG. 7: **Simulation results for the synthetic data classification.** (a) The performance of the conventional quantum classifier under the noiseless setting. The label ‘Train_acc’, ‘Valid_acc’, and ‘Test_acc’ refers to the training, validation, and test accuracy, respectively. (b) The simulation results of QAS in the retraining stage under the noiseless setting. (c) The subnet (i.e., the quantum circuit architecture) searched by QAS in the step 3.

We end this subsection by explaining the fierce competition phenomenon encountered in the optimization of QAS. Namely, when the number of supernet is set as 1, some subnets that can achieve high classification accuracies with independently training, will perform poorly in QAS and hence be grouped into bad subnets. To exhibit that QAS indeed searches a set of subnets (quantum circuit architectures) with high classification accuracies, we examine the correlation of the performance of the subnet with independently optimization and training by QAS. In particular, we randomly sample 8 subnets from all possible architectures and evaluate the widely-used Spearman and Kendall tau rank correlation coefficient [48, 49], which are in the range [0, 1] and larger values mean stronger correlations.

For Spearman rho rank correlation coefficient, it is simply the Pearson correlation coefficient between random variable r and s , if we regard \mathbf{r} and \mathbf{s} as two observation vectors of random variable r and s , i.e.,

$$\rho_S = \frac{\text{cov}(r, s)}{\sigma_r \sigma_s}, \quad (\text{D9})$$

where $\text{cov}(\cdot, \cdot)$ is the covariance of two variables, and σ_r (σ_s) refers to the standard deviations of r (s). The explicit form ρ_S yields

$$\rho_S = 1 - \frac{6 \sum_{i=1}^n (\mathbf{r}_i - \mathbf{s}_i)^2}{n(n^2 - 1)}. \quad (\text{D10})$$

	QAS with $W = 1$	QAS with $W = 5$
ρ_S	0.488	0.773
ρ_K	0.113	0.618

TABLE I: **The correlation coefficients.** The label ‘QAS with $W = a$ ’ represents that the number of supernets is set as a .

The Kendall tau rank correlation coefficient concerns the pairwise ranking performance. For any pair $(\mathbf{r}_i, \mathbf{r}_j)$ and $(\mathbf{s}_i, \mathbf{s}_j)$, it is said to be concordant if $(\mathbf{r}_i > \mathbf{r}_j) \wedge (\mathbf{s}_i > \mathbf{s}_j)$ or $(\mathbf{r}_i < \mathbf{r}_j) \wedge (\mathbf{s}_i < \mathbf{s}_j)$; Otherwise, it is discordant. According to the above definition, the explicit form of the Kendall tau rank correlation coefficient is

$$\rho_K = \frac{2}{n(n-1)} \sum_{i < j} \text{sign}(\mathbf{r}_i - \mathbf{r}_j) \text{sign}(\mathbf{s}_i - \mathbf{s}_j), \quad (\text{D11})$$

where $\text{sign}(\cdot)$ represents to the sign function.

Table I summarizes the correlation coefficients with setting $n = 8$. Specifically, when the number of supernet is 1, the performance of the subnet with independently optimization and training by QAS is almost uncorrelated. By contrast, with increasing the number of supernets to 5, the correlation, evaluated by ρ_S and ρ_K , are dramatically enhanced. These results indicate the competition phenomenon in QAS can be alleviated by introducing more supernets. In doing so, the subnets evaluated by QAS can accord with their true performances with independently training.

E. More results about the ground state energy estimation

In this section, we first briefly recap the ground state energy estimation task in Appendix E 1. We then compare the performance of QAS and conventional VQE towards the ground state energy estimation task when they are implemented on real quantum hardware in Appendix E 2.

1. The ground state energy estimation

A central application of VQLS based algorithms is solving the electronic structure problem, i.e., finding the ground state energies of chemical systems described by Hamiltonians. Note that chemical Hamiltonians in the second quantized basis set approach can always be mapped to a linear combination of products of local Pauli operators [50]. In particular, the explicit form of the molecular hydrogen Hamiltonian H_h in Eqn. (7) is given below, i.e.,

$$H_h = -0.042 + 0.178(Z_0 + Z_1) + -0.243(Z_2 + Z_3) + 0.171Z_0Z_1 + 0.123(Z_0Z_2 + Z_1Z_3) + 0.168(Z_0Z_3 + Z_1Z_2) + 0.176Z_2Z_3 + 0.045(Y_0X_1X_2Y_3 - Y_0Y_1X_2X_3 - X_0X_1Y_2Y_3 + X_0Y_1Y_2X_3). \quad (\text{E1})$$

The goal of variational Eigen-solver (VQE) is generating a parameterized wave-function with

$$\min_{\theta} |\langle \Psi(\theta) | H_h | \Psi(\theta) \rangle - E_m|. \quad (\text{E2})$$

The linear property of H_h in Eqn. (E1) implies that the value $|\langle \Psi(\theta) | H_h | \Psi(\theta) \rangle$ can be obtained by iteratively measuring $|\Psi(\theta)\rangle$ using Pauli operators in H_h , e.g., such as $|\langle \Psi(\theta) | \mathbb{I}_8 \otimes Z_0 | \Psi(\theta) \rangle$ and $|\langle \Psi(\theta) | X_0Y_1Y_2X_3 | \Psi(\theta) \rangle$. The lowest energy of H_h equals $E_m = -1.136$ Ha, where Ha refers to the abbreviation of Hartree, i.e., a unit of energy used in molecular orbital calculations with $1 \text{ Ha} = 627.5 \text{ kcal/mol}$. The exact value of E_m is acquired from a full configuration-interaction calculation [50].

We note that the quantum natural gradient optimizer [51], which can accelerate the convergence rate, is adopted to optimize the trainable parameters for both VQE and QAS, where the learning rate is set as 0.2.

2. The performance of QAS on real quantum devices

Here we carry out QAS and conventional VQE on IBM’s 5-qubit quantum chips, i.e., ‘IBM_ourense’, to accomplish the ground state energy estimation of H_h . The protocol of ‘IBM_ourense’ is illustrated in Figure 8 (a). The connectivities and performances of five qubits are summarized in Table II.

The implementation detail is as follows. In the training process, we leverage the noisy model offered by Qiskit package, which approximates the quantum gates error and readout error in ‘Ibmq_ourense’, to optimize the trainable parameters in VQE and QAS on classical computers. Moving the training stage on the classical numerical simulations is prohibited by the fact that training VQE and QAS on ‘Ibmq_ourense’ will take an unaffordable runtime, due to the fair share run mode [38]. The hyper-parameters settings are $W = 10$, $K = 500$, and $T = 400$. The training performance of VQE and QAS is demonstrated in Figure 8 (c). Particularly, the estimated energy for VQE converges to -1.02 Ha after 30 iterations, highlighted by the dark blue line. When we retrain the searched subnet of QAS with 50 iterations, its estimated energy converges to -1.06 Ha, highlighted by pink solid line. The circuit layout of the search subnet is shown in Figure 8 (b). Compared with the searched subnet in the main text, this subnet contains more CNOT gates. This implies that when the two qubits gate error is not too large, QAS prefers to add more two qubits gates to increase the expressive power of trainable circuit. The ranking distribution of the sampled 500 subnets is shown in Figure 8 (b). For most subnets, their estimated energies are above -0.2 Ha.

After training, we implement VQE and the subnet search by QAS associated with their optimized parameters on ‘Ibmq_ourense’ to test their estimated energies. The experimental results are illustrated in Figure 8 (b). Specifically, the test ground energy for VQE is only -0.61 Ha, while the test ground energy for QAS is -0.865 Ha. The varied numerical and experimental performances are caused by that the noisy model can not exactly capture all imperfections

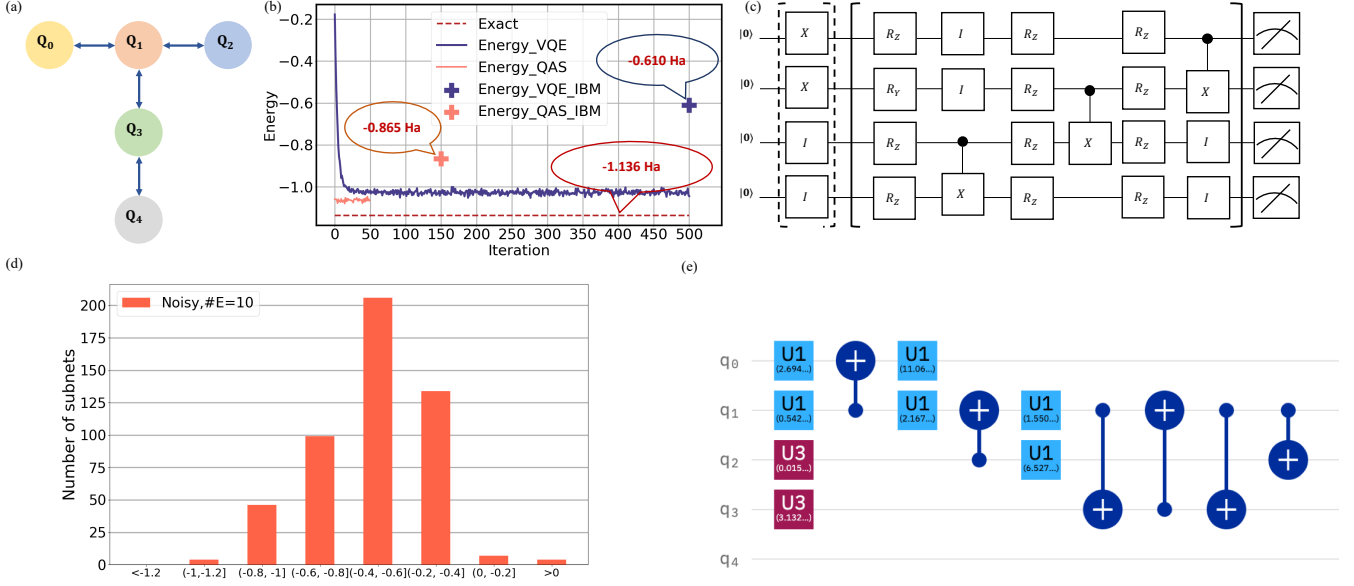


FIG. 8: **Simulation results of the ground state energy estimation.** (a) The qubits connectivity of 'IBM_ourense'. (b) The training performance of VQE and the subnet searched by QAS. The labels 'Exact', 'Energy_VQE', 'Energy_QAS', 'Energy_VQE_IBM', and 'Energy_QAS_IBM' refer to the exact ground state energy, the estimated energy of VQE and QAS in the training process implemented on numerical simulations, and the estimated energy of VQE and QAS in the test stage implemented on 'IBM_ourense'. (c) The quantum gates arrangement of the searched subnet. (d) The 500 subnets ranking distributions. The x-axis refers to the estimated energy of the given subnet is in the range of $(a \text{ Ha}, b \text{ Ha}]$ with $a, b \in \mathbb{R}$. (e) The implementation of the searched subnet on 'IBM_ourense'.

Qubit	T1(μs)	T2(μs)	Readout error	Single-qubit U2 error gate	CNOT error rate
Q0	75.75	50.81	1.65E-2	5.22E-4	cx0-1: 9.55E-3
Q1	78.47	27.56	2.38E-2	4.14E-4	cx1-0: 9.55E-3 cx1-2: 9.44E-3 cx1-3: 1.25E-2
Q2	101.51	107.00	1.57E-2	1.83E-4	cx2-1: 9.44E-3
Q3	79.54	78.38	3.95E-2	4.30E-4	cx3-1: 1.25E-2 cx3-4: 8.34E-3
Q4	74.27	30.00	4.74E-2	4.20E-4	cx4-3: 8.34E-3

TABLE II: **Performance of qubits for the Ibmq_ourense.** T1 and T2 refer to the energy relaxation time and dephasing time, respectively. U2 and CNOT gates error obtained via performing randomized. The label 'cxa-b' represents that the CNOT gate is applied to the qubits a and b .

in 'Ibmq_ourense'. Despite the discrepancy, QAS achieves a lower energy than that of VQE. This result implies the effectiveness of QAS towards quantum chemistry tasks.